The calcination temperature dependence of microstructural, vibrational spectra and magnetic properties of nanocrystalline $Mn_{0.5}Zn_{0.5}Fe_2O_4$

The calcination temperature dependence of microstructural, vibrational spectra and magnetic properties of nanocrystalline $Mn_{0.5}Zn_{0.5}Fe_2O_4$

I. P. T. Indrayana[1], N. Siregar[1], E. Suharyadi[1*], T. Kato[2] and S. Iwata[3]
[1] Department of Physics, Gadjah Mada University, Yogyakarta, INDONESIA
[2] Department of Electrical Engineering & Computer Science, Nagoya University
[3] Institutes of Materials and Systems for Sustainability, Nagoya University, JAPAN

*E-mail: esuharyadi@ugm.ac.id

Abstract. Effect of calcination temperature on microstructural, vibrational, and magnetic properties of $Mn_{0.5}Zn_{0.5}Fe_2O_4$ nanoparticles have been successfully investigated. The nanoparticles were synthesized via coprecipitation method and calcined at different temperatures varying from 400, 600, 800, and 1000°C. The X-ray diffraction (XRD) pattern confirmed the formation of cubic spinel structure $Mn_{0.5}Zn_{0.5}Fe_2O_4$ with crystallite size ranging from 18.3 nm to 24.8 nm. The TEM micrograph showed the morphology of nanoparticles change from nearly spherical to cubic form after calcination. The FTIR spectra confirmed the existence of vibrations at 416.6 cm^{-1} - 455.2 cm^{-1} and 555.5 cm^{-1} -578.6 cm^{-1} which corresponds to the intrinsic stretching vibration of metal-oxygen at octahedral and tetrahedral sites, respectively. The maximum specific magnetization and coercivity increase with increasing calcination temperature. The maximum specific magnetization value of 54.7emu/gram was obtained for sample calcined at 1000°C. The results showed that calcination treatment will facilitate the tunability of microstructural and magnetic properties of nanoparticles for expanding the field of application.

1. Introduction

Spinel ferrite nanoparticles with molecular equation MFe_2O_4 (M: Mn^{2+}, Zn^{2+}, Fe^{2+}, Co^{2+}, Ni^{2+}, etc.) are very promising nanomaterial which have many practical applications such as transducers, transformers and electromagnetic interference shielding materials due to their high electrical resistivity and dielectric constant [1]. Meanwhile, because of their high magnetic properties as well as unique crystal and electronic structure allow ferrite nanoparticles to be utilized as high-density information storage media, magnetic printing inks, magnetic drug delivery and magnetic resonance imaging (MRI) enhancement [2,3]. In recent years, spinel ferrite nanoparticles have been also achieved great attention as photocatalyst materials. In this context, ferrite nanoparticles offer several advantages of having narrow band gap for example 1.25 eV for $MnFe_2O_4$ and 1.30 eV for $ZnFe_2O_4$ [4] and high magnetic properties that allow to the development of magnetic separation technology which is very effective, simple, and low cost process compare to centrifugation and filtration [5]. Those advantages can overcome the drawback of TiO_2 and ZnO nanoparticles that are common photocatalyst material have been used. Therefore, in other to obtain high quality photocatalyst materials so engineering ferrite nanoparticles with different metal ion composition, surface modification and synthesis method are the three important efforts that being focussed by researchers up to the present. For example, Ibrahim *et al*. [4] had engineered $MnFe_2O_4$ and $ZnFe_2O_4$ by sol-gel hydrothermal technology to investigate the photocatalytic activity of these ferrite nanoparticles for nitroarenes reduction.

$Mn_{0.5}Zn_{0.5}Fe_2O_4$ ferrite nanoparticles have been long studied for their high magnetic properties. This nanoparticles were formed by introduce nonmagnetic Zn^{2+} ion to $MnFe_2O_4$. Many researchers have varied the molar composition for both Mn^{2+} and Zn^{2+}. The composition of $Mn_{0.5}Zn_{0.5}Fe_2O_4$ gave the most stable magnetic properties [6,7]. Naik *et al*. [6] had found that $Mn_{0.5}Zn_{0.5}Fe_2O_4$ nanoparticles have specific magnetization saturation of 40.65 emu/gram and coercivity of 113.78 Oe. Meanwhile, Baykal *et al*. [7] revealed the band gap of $Mn_{0.5}Zn_{0.5}Fe_2O_4$ nanoparticles in range of 2.60 eV - 2.80 eV. Both magnetic properties and band gap of nanoparticles are influenced by the crystal structure, crystallite size and microstructure of grain nanoparticles.

In regard to obtain good microstructure of nanoparticles, synthesis procedure and heat treatment play important role [8-11]. Therefore, in the present research $Mn_{0.5}Zn_{0.5}Fe_2O_4$ were synthesized via coprecipitation method. Coprecipitation has very simple procedure. The synthesized nanoparticles have small crystallite size [12]. Unfortunately, this method have significant drawback such as the nanoparticles have broad crystallite size distribution and the small size make the nanoparticles tend to agglomerate that causes the weakening of microstructural and magnetic properties [12]. Therefore, controlling the size distribution and microstructure of nanoparticles via heat treatment such as calcination is needed.

This research was a part of project to engineer magnetic ferrite photocatalysts materials and aimed to control the microstructure and vibrational spectra of $Mn_{0.5}Zn_{0.5}Fe_2O_4$ nanoparticles by varying the calcination temperatures. Hopefully, by involving calcination process after synthesis, the crystallinity and microstructure of nanoparticles can be tuned as well as the magnetic properties.

2. Experimental Method

$Mn_{0.5}Zn_{0.5}Fe_2O_4$ nanoparticles were prepared by chemical coprecipitation method. The materials used were $FeCl_3.6H_2O$, $ZnSO_4.7H_2O$, $MnCl_2.H_2O$, HCl and NaOH. All the chemicals were of analytical grade (Merck Emsure) and used without any further purification. The chemical reaction is described by

$$\begin{aligned} &4FeCl_{3(aq)} + MnCl_{2(aq)} + ZnSO_{4(aq)} + 16NaOH_{(aq)} + 2H_2O_{(aq)} \\ &\qquad\qquad \downarrow + HCl_{(aq)} \\ &2Mn_{0.5}Zn_{0.5}Fe_2O_{4(s)} + 14NaCl_{(aq)} + Na_2SO_{4(aq)} + 10H_2O_{(aq)} \end{aligned} \quad . \qquad 1)$$

First of all, $FeCl_3.6H_2O$ and the combination of $ZnSO_4.7H_2O$ and $MnCl_2.H_2O$ were individually dissolved in 20 ml of distilled water within 2 minutes at room temperature under constant stirring of 500 rpm. Those combined solutions were added of 3.37 ml HCl and mixed within 5 minutes under constant stirring of 500 rpm. The mixture then added dropwise to a boiling of 1.5 M NaOH with pH around 12 throughout burette. Nanoferrites are formed by conversion of metal salts into hydroxides, which takes place immediately and the transformation of hydroxides into ferrites. The solutions were maintained at 120^{o}C under constant stirring of 1000 rpm for 60 minutes. This duration was sufficient for the transformation of hydroxides into spinel ferrite (dehydration and rearrangement involved in the conversion of intermediate hydroxide phase into ferrite). The dark precipitates were obtained and then cooled to a moderate temperature. The precipitates were washed for 6 times using distilled water. The slurries of nanoparticles were obtained through filtration and continued washing by acetone for 2 times. The filtered particles were dried at 90^{o}C in a furnace for 4 hours. Finally, the fine powders were yielded and calcined with four difference temperatures i.e., 400^{o}C, 600^{o}C, 800^{o}C and 1000^{o}C.

The composition and crystallite structure of powder nanoparticles were analysed by X-Ray diffractometer Shimadzu XD using monochromic Cu-Kα radiation (λ = 1.5406 Å). The average crystallite size was calculated by applying peak broadening of (311) using Scherer's equation [13]. The vibrational spectra of nanoparticles were recorded by Fourier transform infrared spectroscope (FTIR) Prestige Shimadzu-21 in range of 4000 – 400 cm^{-1}. The morphology and selected area diffraction (SAED) pattern were performed by Transmission electron microscope (TEM) Jeol Jem-1400. The room temperature magnetic properties measurement of sample nanoparticles was carried out by using Vibrating sample magnetometer (VSM) Riken Denshi Co Ltd.

3. Results and Discussion

3.1 XRD analysis

Figure 1 shows the XRD pattern of calcined and as prepared $Mn_{0.5}Zn_{0.5}Fe_2O_4$ nanoparticles at difference temperatures. The patterns show the characteristic peaks of cubic spinel structures, such as (220); (311); (400); (422); (511); and (440) according to JCPDS (10-0467). The peaks are broad and low intensity that confirm still the low crystallinity of sample nanoparticles. The intensity of nanoparticles increases with an increase of calcination temperature. The peak of (311) shifts to the lower diffraction angle due to increase of calcination temperature that causes strain on crystal lattice of nanoparticles [14]. The lattice exhibits expansion during calcination that makes change ions position in entire crystal lattice, so the interplanar distance of diffraction planes tend to be larger.

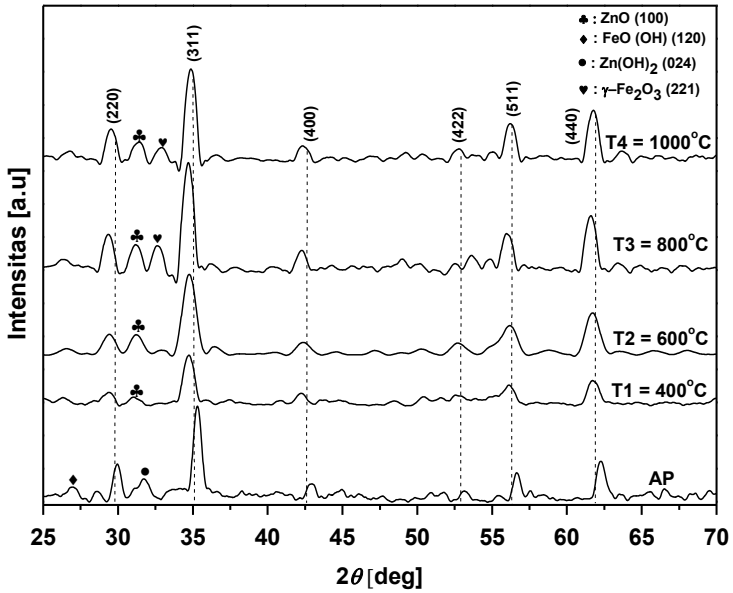

Figure 1. XRD pattern of $Mn_{0.5}Zn_{0.5}Fe_2O_4$ nanoparticles for various temperature: AP (as prepared nanoparticles); T1 (400°C); T2 (600°C); T3 (800°C); and T4 (1000°C)

XRD patterns also confirm the existence of nonspinel $Mn_{0.5}Zn_{0.5}Fe_2O_4$ phase (Table 1), such as $Zn(OH)_2$ (JCPDS no. 01-0360); FeO(OH) (JCDPS no. 17-0536) for as prepared sample and ZnO (JCPDS no. 36-1451) as well as γ-Fe_2O_3 (JCPDS no. 39-1346) for calcined samples. The appearance of $Zn(OH)_2$ and FeO(OH) are considered caused by incomplete ferritization process of precipitated salt precursors to form spinel $Mn_{0.5}Zn_{0.5}Fe_2O_4$ phase. In other hand, the appearance of ZnO and γ-Fe_2O_3 might be caused by thermal decomposition of unreacted $Zn(OH)_2$ and FeO(OH) during calcination. According to thus data can be predicted that the real composition of $Mn_{0.5}Zn_{0.5}Fe_2O_4$ will deviate from the analytical stoichiometry. Therefore, the cationic distribution of nanoparticles will change and influence the crystallite size and lattice parameter [15].

Table 1. Phase compostion of $Mn_{0.5}Zn_{0.5}Fe_2O_4$ nanoparticles

Sample	Spinel phase composition (%)	Nonspinel composition (%)			
		ZnO	$Zn(OH)_2$	FeO(OH)	γ-Fe_2O_3
AP	86.30	-	7.85	5.85	-
T1	94.41	5.59	-	-	-
T2	96.84	3.16	-	-	-
T3	77.88	9.06	-	-	13.06
T4	84.36	6.89	-	-	8.75

The crystallite size and lattice parameter of nanoparticles can be presented in Table 2. The crystallite size tends to increase with an increase of calcination temperature due to grain growth of nanoparticles. The lattice parameter of nanoparticles does not show certain trend due to deviation of cation distribution in both sites of tetrahedral and octahedral caused by thermal fluctuation. The values are higher than that of theoretical calculation, except for as prepared sample. The theoretical calculation based on the following cation distribution and the equation given by [16],

$$(Mn_{0.4}^{2+}Zn_{0.5}^{2+}Fe_{0.1}^{3+})_{tet}\,[Mn_{0.1}^{2+}Fe_{1.9}^{3+}]_{oct}O_4^{2-}.$$

Table 2. Structural parameters of $Mn_{0.5}Zn_{0.5}Fe_2O_4$

Structural Parameter / Sample	AP	T1	T2	T3	T4
Crystallite size (nm) (± 0.2)	21.4	21.9	18.3	24.8	22.3
Lattice parameter (Å)	8.424	8.562	8.540	8.565	8.525
Theoretical Lattice parameter (Å)	8.478	8.478	8.478	8.478	8.478
Difference of lattice parameter (%)	0.63	0.99	0.73	1.03	0.55
Lattice strain ($\times 10^{-4}$ /line^2)	16.19	15.85	18.79	13.98	15.52
Specific surface area ($\times 10^{-1}$ m^2/kg)	53.48	54.97	65.30	48.53	53.14

The lattice strain of nanoparticles tends decrease with an increase of calcination temperature. Thus confirm that the crystallinity of nanoparticle increase. Hence, increase the crystallite size makes the specific surface area of nanoparticles decrease. The highest specific surface area was found in sample of calcination temperature 600^{o}C. Technically, for photocatalysis application sample T2 might perform the best catalytic activity because of their crystallinity, the lowest crystallite size and the highest specific surface area for enhancing photoreaction and pollutant degradation.

3.2 TEM analysis

TEM images of nanoparticles can be presented in Figure 2. TEM images show as prepared nanoparticle experience agglomeration due to small crystallite size that produces high surface energy and surface tension of nanoparticles. The grain size calculated from the image was 32.6 ± 0.8 nm which consistent to the XRD result. In other hand, the TEM image of calcined nanoparticles shows the formation of polydisperse grain with morphology changes from nearly spherical into cubic form. The grain of nanoparticles becomes bigger so that the surface energy was reduced as the increase of calcination temperature. The average grain size of nanoparticles was 59.9 ± 0.6 nm. The SAED patterns for both samples confirm nanoparticles were polycrystalline materials.

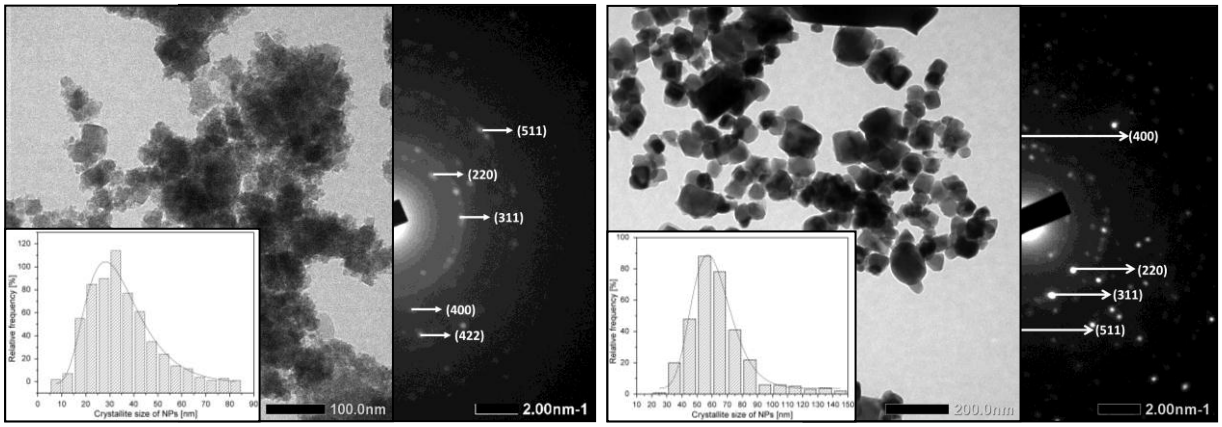

(a) (b)

Figure 2. TEM images of $Mn_{0.5}Zn_{0.5}Fe_2O_4$: (a) as prepared, (b) calcined at 800^{o}C

3.3 FTIR analysis

The FTIR spectra (Figure 3) confirmed the existence of Me_{oct} – O bonds vibration, such as Mn-O and Fe-O stretching bonds in octahedral sites with frequencies of 416.6 cm^{-1} – 455.2 cm^{-1}. The stretching vibration of Me_{tet} – O bonds such as Mn-O; Zn-O and Fe-O were identified in frequencies of 555.5 cm^{-1} – 578.6 cm^{-1}. Increasing the calcination temperature causes shift of frequencies toward smaller values due to the change of cation distribution and bond length between cation- anion in crystal lattice. The Fe-O-H bending vibration occurs in frequencies of 1080.1 cm^{-1} – 1126.6 cm^{-1}. This group might appear from FeO(OH) and hydration of γ-Fe_2O_3 that have been showed in XRD data.

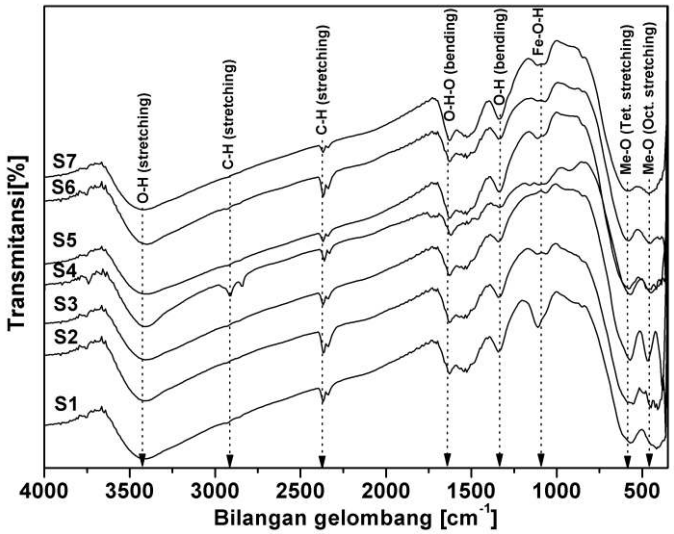

Figure 3. Vibrational spectra of $Mn_{0.5}Zn_{0.5}Fe_2O_4$ nanoparticle for various calcination temperatures

The vibration in frequencies of 1342.5 cm^{-1} and 1627.9 cm^{-1} correspond to O-H and H-O-H stretching bonds which are considered appear from the KBr materials that very hygroscopic to react with oxygen and hydrogen in atmosphere during samples preparation. The appearance of asymmetric stretching vibration of C-H in frequencies of about 2337.7 cm^{-1} and 2916.4 cm^{-1} – 2931.8 cm^{-1} were considered as result of chemical reaction between nanoparticles and CO_2 and H_2 in atmosphere [17].

3.4 VSM analysis

Magnetic parameters of nanoparticles can be presented in Table 3 and Figure 4. The coercivity tends increase with an increase of calcination temperature. The increase in coercivity is a direct result of increase in crystallite size [18]. During calcination nanoparticles experience grain growth and nucleation so that crystal lattice also experience thermal expansion. Thermal energy triggers the driving forces of nanoparticles to decrease their surface energy. The surface spin of nanoparticles will resist their position by enhancing magnetocrystalline anisotropy therefore the coercivity becomes higher. The lower coercivity of sample T3 then T2 might be caused by the existence of ZnO and γ-Fe_2O_3 phases which exhibit diamagnetic and antiferromagnetic properties, respectively.

Table 3. Magnetic properties of prepared and calcined $Mn_{0.5}Zn_{0.5}Fe_2O_4$ nanoparticles

Sample	Crystallite size (± 0.2 nm)	*Hc* (Oe)	σ_r (emu/grm)	σ_{max} (15 kOe) (emu/grm)
S4	21.4	47.4	1.0	10.4
T1	21.9	28.2	0.0	24.1
T2	18.3	110.9	0.9	28.7
T3	24.8	104.7	0.5	23.7
T4	22.3	154.5	6.1	54.7

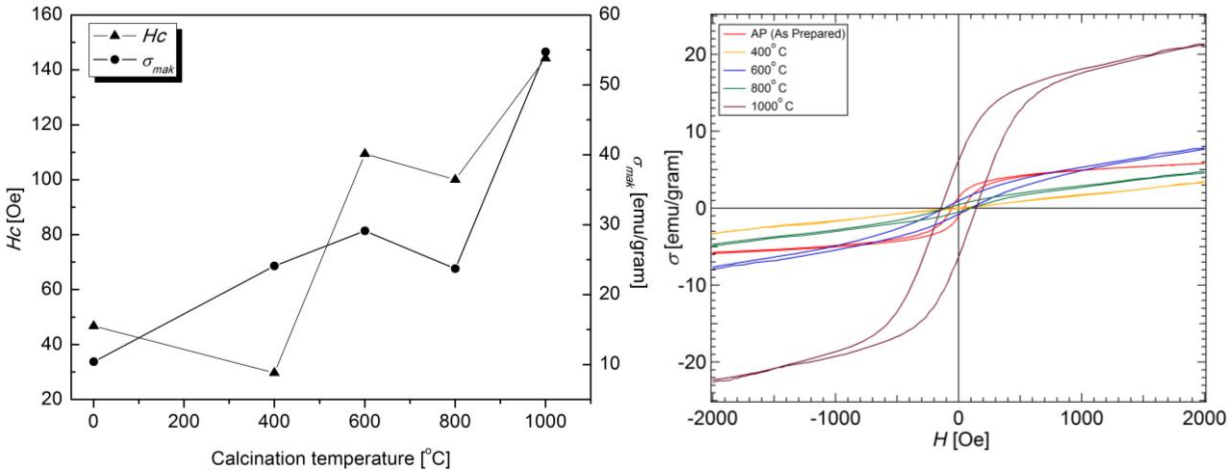

Figure 4. Magnetic properties and the hysterisis loop of $Mn_{0.5}Zn_{0.5}Fe_2O_4$ nanoparticles

Samples of nanoparticles have small specific remanence magnetization due to random canting of particles surface spins [12]. The specific maximum magnetization of nanoparticles tends to increase with an increase of calcination temperature. The values are in range of 10.4emu/gram - 54.7emu/gram. The increase might be attributed by increase of crystallite size that followed by the motion of magnetic domain wall in entire nanoparticles. As the calcination temperature increase, domain wall motion will increase rapidly. The motion of domain wall will contribute to the value of specific maximum magnetisation under external magnetic field of 15 kOe.

4. Conclusion

The $Mn_{0.5}Zn_{0.5}Fe_2O_4$ nanoparticles have been successfully synthesized via coprecipitation. The calcination treatment was proved facilitate the tunability of microstructural, crystal structure, vibrational spectra and magnetic properties of nanoparticles. The calcination treatment of 1000°C results the highest magnetic properties of nanoparticles with the highest quality of microstructure.

5. Acknowledgement

The reported work was financially supported by LPDP Thesis Scholarship 2016 and Nanofabrication Platform Consortium Project of Nagoya University, Minister of Culture, Sports, Science and Technology (MEXT) Nano-Project Platform, Japan of Period 2012 - 2016.

6. References

[1] Choodamani, C., Nagabhushana, G.P and Chandrappa, G.T 2014 *Mater. Lett*. 116 p. 227–230
[2] Gharagozlou, M 2009 *J. Alloys.Compd*. 486 p 660–665
[3] Issa, B., Ihab, M., Obaidat, Albiss, B.A and Haik, Y 2013 *Int. J. Mol. Sci*. 14 p 21266-21305
[4] Ibrahim, I., Ali, I., Salama, T.M., Bahgat and Mohamed, M.M 2016 *App. Catalysis B*. 181 p 389–402
[5] Pang, Y.L., Lim, S., Ong, H.C and Chong, W.T 2006 *Ceramics International*. 42 p 9–34
[6] Naik, P.P., Tangsali, R.B., Sonaye, B and Sugur, S 2015 *J. Magn. Magn. Mater*. 385 p 377–385
[7] Baykal, A., Güner, S and Demir, A 2015 *J. Alloys. Compd*. 619 p 5–11
[8] Gharagozlou, M 2009 *J. Alloys. Compd*. 486 p 660–665
[9] Sharifi, I and Shokrollahi, H 2012 *J. Magn. Magn. Mater*. 324 p 2397–2403
[10] Augustina, M and Balu, T 2015 *Mater. Today: Proc*. 2 p 923 – 927
[11] Reddy, C.V., Vattikuti, S., Ravikumar, Moon, S and Shim, J 2015 *J. Magn. Magn. Mater*. 394 p 70–76
[12] Lan, N.T., Hien, T.D., Duong, N.P and Truong, D.V 2008 J. *the Korean Phys. Soc*. 52 p 1522 – 1525
[13] Amirabadizadeh, A., Farsi, H., Dehgani, M and Arabi, H 2012 *J. Superc. Novel Magn*. 25 p 2763 – 2765
[14] Zak, A.K., Majid, W.H., Abrishami, M.E and Yousefi, R 2011 *Solid State Scie*. 13 p 251-256

[15] Rath, C., Anand, S and Das, R.P 2001 *J. App. Phys*. 91 p 2211 – 2215
[16] Mohammed, K.A., Rawas, A.D., Gismelseed, A.M., and Shongwe, M 2012 *Physica B*. 407 p 795–804
[17] Larkin, P.J 2011 *IR and Raman Spectroscopy: Principles and Spectral Interpretation* (USA: Elsevier) p 38
[18] Vaidyanathan, G., Arulmurugan, R., Likhite, S.D and Anantharaman, M.R 2004 *Ind. J. Eng. Mater. Scie*. 11 p 289 – 294